Angle-resolved photoemission study of the clean Cu (001) surface in the photon energy range $40 \leq \hbar\omega \leq 120$ eV: Comparison of experiment and simple direct-transition theory

Z. Hussain,* S. Kono, L.-G. Petersson,† C. S. Fadley,‡ and L. F. Wagner
Department of Chemistry, University of Hawaii, Honolulu, Hawaii 96822
(Received 15 January 1980)

Angle-resolved photoemission spectra obtained from the clean Cu (001) surface with photon energies in the range 40–120 eV and emission both normal and non-normal to the surface are well predicted by a simple constant-matrix-element model based upon direct ($\vec{k}$ conserving) transitions between initial electronic states with full bulk translational symmetry and final states with a free-electron dispersion relation and a correction for refraction at the crystal surface. In addition, the quantitative agreement between theory and experiment improves significantly by including broadening in the final-state wave vector for spectra obtained in the highly-surface-sensitive region around 100 eV. A strong contribution of phonon-assisted indirect transitions to the spectra also appears to be present. The photoemission spectra have been obtained at two different polarization orientations with respect to the electron emission direction and this can be used for assigning contributions from various initial states.

I. INTRODUCTION

Numerous angle-integrated[1-3] and angle-resolved[2,4-12] photoemission studies have been performed on clean surfaces of copper single crystals to determine the electronic structure of this material and also to elucidate the underlying theory of the photoemission process. Because of its rather noble character and quite accurately known theoretical band structure,[13,14] copper has often served as a model for interpreting photoemission spectra.[1,2,5-12,15] By now, it has been demonstrated in several studies[1,4,5,15] that a direct-transition model in which $\vec{k}$ is rigorously conserved can be utilized successfully for interpreting the photoemission spectra at conventional ultraviolet photoelectron spectroscopy (UPS) energies of $\lesssim 20$ eV. More recently, Wagner *et al.*[9] applied a bulk direct-transition model requiring conservation of energy and wave vector and neglecting matrix-element variations to angle-resolved data obtained by Stöhr *et al.*[6] in the intermediate energy range of $30 \lesssim \hbar\omega \lesssim 200$ eV. They showed that this simple model, which further assumes a strictly free-electron-like final-state band structure, predicts correctly the photon-energy-dependent normal photoemission spectra from Cu (001) and Cu (111). This work has been followed by other studies in the same energy range by Stöhr *et al.*[10] and Thiry *et al.*,[12] and it has been established that this direct-transition model indeed can rather well predict most of the structures observed in *normal* photoemission spectra in this intermediate energy range. The range of validity of direct transitions has also been discussed by Shevchik, who studied the role of phonon-assisted indirect transitions in the photoemission process.[16] According to this work,[16] there are two contributions to the photoemission spectra: one from direct ($\vec{k}$ conserving) transitions and other from phonon-assisted indirect transitions, with the latter becoming more significant at high temperatures and/or high photon energies. This observation can explain why the direct-transition model works so well at low energies, but not as well in the x-ray region.[16,17] An alternative explanation of the breakdown of the simple direct-transition model at higher energies as being due to final electronic-state complexity has been discussed by Sayers and McFeely,[18] but this is not consistent with recent temperature-dependent x-ray photoemission measurements on W by Hussain *et al.*[19]

We have thus been prompted by the successful application of this direct-transition model to normal photoemission at intermediate energies to undertake a systematic study of the clean Cu (001) surface in the energy range $\hbar\omega = 40$–120 eV with both normal and off-normal emission. An important point of interest is thus whether the momentum-conserving selection rule can be simply applied for both normal and non-normal emission in this energy range, provided that possible electron refraction effects at the surface are allowed for.[20] In fact we find that the rule applies rather well for both cases. Thus, by utilizing emission directions both normal and non-normal to the surface along with $\vec{k}$-conserving transitions, it is possible to select energies and emission directions for one crystal-surface orientation that correspond to emission from initial states near various symmetry points in the Brillouin zone. Prior angle-resolved experiments in this energy range had been mostly limited to normal photoemission

and thus also to mapping along only a single direction in the Brillouin zone for each surface orientation.[2,9,12] The experiments were also performed at two different orientations of the polarization vector ($\vec{A}$) relative to the electron emission direction and the spectral changes thus noted can be related to the known symmetries of the initial and final states. Also, inasmuch as the energy range utilized encompasses the region of minimum mean free path expected at ~60–100 eV,[21] we have in analyzing our data considered several effects such as final-state momentum broadening[2,12,22-24] (which appears to be important for this case) and surface states[25-27] and surface umklapp scattering[12,22] (which do not appear to be important). In addition, it has been possible to infer the existence of phonon-assisted indirect transitions by exciting initial states near equivalent Brillouin-zone symmetry points with photon energies of nearly equal surface sensitivity but for which different $\vec{g}$ vectors are involved in the direct transitions. Finally, in a separate part of this general program of study, we have also performed angle-resolved photoemission experiments of the same type for Cu (001) with a $c(2\times2)$ oxygen overlayer, and these are discussed elsewhere.[28]

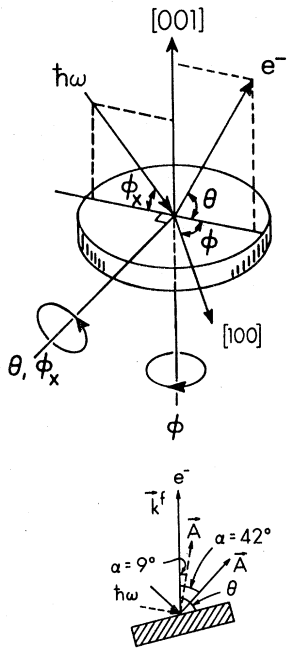

FIG. 1. Schematic diagrams showing the experimental geometry and the two polarization directions used. The angle α between the electron propagation and the polarization vector $\vec{A}$ was fixed at either 9° or at 42°. Rotation of the specimen on both the θ and ϕ axes was possible.

II. EXPERIMENTAL PROCEDURE

The angle-resolved photoemission experiments were carried out on the 4° beam line of the Stanford Synchrotron Radiation Laboratory using photon energies in the range of 40–170 eV. Schematic diagrams of the experimental geometry are shown in Fig. 1. Polar rotations were performed about an axis perpendicular to a plane containing the polarization vector $\vec{A}$ and the electron propagation direction. Azimuthal rotations were about the surface normal. The polar angle, θ, was measured with respect to the surface such that 90° corresponded to emission perpendicular to the surface. The azimuthal angle ϕ was arbitrarily measured with respect to the [100] crystal direction. A commercial double-pass cylindrical mirror analyzer (CMA) was modified for angle-resolved measurements by the addition of an aperture resulting in an electron acceptance angle of $10°\times12°$. The polarized monochromatic synchrotron radiation was directed onto the specimen at two different orientations such that the angle α between the electron emission direction and the polarization vector $\vec{A}$ could be chosen to be either 9° or 42° (Fig. 1). This change in the orientation of $\vec{A}$ with respect to the electron emission direction was affected by rotating the sample chamber and admitting the radiation through two different ports, a movement that was possible without breaking the vacuum in the chamber. For both orientations, the polarization vector $\vec{A}$ lay in the plane defined by both the propagation direction of the light beam and the normal to the specimen surface (i.e., the incident light was generally p polarized). The analyzer system was combined with a specially-built broad-temperature-range sample manipulator which permitted directional analysis of the photoemitted electrons over the entire range of polar and azimuthal angles with accuracies of approximately ±0.5°.

The sample was cut from a bulk single crystal and was oriented to within ±0.5° of the (001) surface. The crystal was polished using standard mechanical techniques and was chemically etched to remove surface disorder introduced by the mechanical polishing. The sample was cleaned *in situ* by argon-ion bombardment and annealed at temperatures in the range 500–600 °C to remove surface damage. Electron-excited Auger spectra were used for monitoring the cleanliness of the surface. Carbon was the principal contaminant and it was present in an amount corresponding to less than a few percent of a monolayer. Operating pressures during all the measurements were $\lesssim 2\times10^{-10}$ Torr. A low-energy electron diffraction (LEED) system was also mounted on the chamber; this was used to verify good surface order

and orientation. All the valence-band spectra were recorded at a CMA pass energy of $E_p = 50$ eV, corresponding to a spectrometer resolution of ~0.3 eV. The monochromator contribution to linewidths varied from ~0.03 eV at $\hbar\omega = 40$ eV to ~0.23 eV at $\hbar\omega = 120$ eV. All electron binding energies reported here are relative to the Fermi energy, and the azimuthal and polar angles utilized are indicated on each spectrum shown below. The data were initially obtained in channels of 0.03 eV in width, but it has subsequently been smoothed by doing least-squares polynomial fits[29] of second order over 15 points or a range of 0.45 eV.

III. THEORY

A. Direct-transition model

The theoretical calculations used for interpreting these angle-resolved photoemission spectra were performed using two slightly different direct-transition models. In the first set of calculations, a model identical to that applied previously by Wagner *et al.*[9] for the interpretation of normal photoemission spectra from Cu (001) and Cu (111) in the energy range 32-200 eV was used. Here we briefly summarize this simple model as applied to our work. In general the photoelectron energy distribution $N(E,\hbar\omega)$ is given in a simple one-electron picture by[23,30]

$$N(E,\hbar\omega) \propto \int_{\vec{k}^i} \int_{\vec{k}^f_{\rm obs}} d^3k^i d^3k^f \left| \langle \phi^f(\vec{r}) | \vec{A}\cdot\vec{\nabla} | \phi^i(\vec{r}) \rangle \right|^2 \times \delta(\vec{k}^f - \vec{k}^i - \vec{k}_{\hbar\omega} - \vec{g}) \times \delta(E^f - E^i - \hbar\omega)\delta(E - E^i) , \quad (1)$$

in which $\phi^f(\vec{r})$ and $\phi^i(\vec{r})$ are the final and initial electronic wave functions, $\vec{k}^f$ and $\vec{k}^i$ are the final and initial electron wave vectors, $\vec{A}\cdot\vec{\nabla}$ represents the perturbation due to the radiation, $\vec{k}_{\hbar\omega}$ is the photon wave vector (with $k_{\hbar\omega} = \omega/c$), and $\vec{g}$ is a reciprocal-lattice vector. $\vec{k}^f$ is expressed in an extended-zone scheme and $\vec{k}^i$ in a reduced-zone scheme (cf. Fig. 2). The delta functions account for wave-vector conservation and energy conservation. That for $\vec{k}$ also includes $\vec{k}_{\hbar\omega}$ for complete generality, as it becomes non-negligible in comparison to $\vec{k}^i$ (reduced) at energies as high as those used in x-ray photoelectron spectroscopy (XPS) experiments,[8,19] although $\vec{k}_{\hbar\omega}$ is generally a very small correction for the energies considered here. The integral in $\vec{k}^f$ is over observed $\vec{k}^f$ values whose directions span a rectangular solid angle with overall dimensions of $10°\times 12°$ for the present experimental geometry. The integration on $\vec{k}^i$ is over all occupied initial states. Because band-structure calculations at high energies for copper are not yet available, the simplifying assumption that the magnitude of $\vec{k}^f$ inside the crystal can be estimated with sufficient accuracy by using the free-electron expression $|\vec{k}^f| = (2mE^f/\hbar^2)^{1/2}$ is made. The applicability of such a free-electron dispersion relation has also recently been demonstrated by Nilsson *et al.*[31] for Cu at even lower excitation energies of 16.6–21.2 eV, and they have discussed one likely reason for this: the inclusion of damping due to inelastic scattering in the description of the final state. As to the matrix elements $\langle \phi^f | \vec{A}\cdot\vec{\nabla} | \phi^i \rangle$, it has been shown previously by Wagner *et al.*[9] that the inclusion of matrix elements based on the simple expediency of the plane-wave final-state approximation $\phi^f = \exp(i\vec{k}\cdot\vec{r})$ results in very poor agreement between theory and experiment. Therefore, because any more accurate treatment of matrix elements would complicate these calculations considerably, they are assumed to be constant for all transitions. In our calculations, the initial-state band structure $E^i(\vec{k}^i)$ is obtained by a second-order Taylor-series interpolation of the tabulated bulk band structure of copper by Burdick.[13]

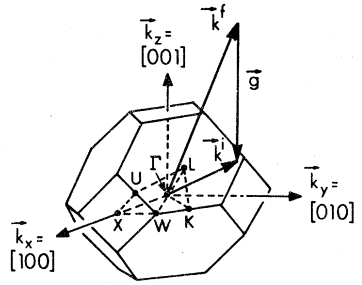

FIG. 2. Schematic illustration of the direct-transition model utilized to select different initial states for study. The first Brillouin zone for fcc Cu is shown with various symmetry points and lines.

In order to associate the wave vector $\vec{k}^f$ inside the crystal with the observed free-electron wave vector $\vec{K}^f$ outside the crystal, it is necessary to include possible refraction effects for the escaping photoelectrons as they interact with the surface potential barrier V_0.[22,30] With simple free-electron states inside and outside and the assumption of specular boundary conditions, $\vec{k}^f$ is related to $\vec{K}^f$ by the following relations for components parallel and perpendicular to the surface:

$$\vec{k}^f_{\parallel} = \vec{K}^f_{\parallel} , \quad (2)$$

$$(\hbar^2/2m)\,|\vec{k}^f_{\perp}|^2 = (\hbar^2/2m)\,|\vec{k}^f_{\perp}|^2 - V_0 . \quad (3)$$

V_0 is the inner potential and is taken to be the energy difference between the bottom of the copper valence band and the vacuum level. Utilizing the above expression, the angle θ of the emerging photoelectrons with respect to the surface becomes

$$\theta = \arccos\{[(E_{\text{kin}} + V_0)/E_{\text{kin}}]^{1/2}\cos\theta'\}, \quad (4)$$

where θ' is the angle with respect to the surface of the propagating electrons inside the crystal, and E_{kin} is the energy of the photoelectrons with respect to the vacuum level. Such refraction effects were calculated from Eq. (4) by using an inner potential of 14.1 eV [the sum of the theoretical 8.98-eV Fermi energy[13] and the 5.16-eV work function for the copper (001) face[32]]. This value of V_0 also agrees rather well with an empirical result of 13.8 eV obtained by Thiry *et al.*[12] in comparing normal emission data with direct-transition theory. The refraction thus calculated was included in making all of our experimenal settings and is $\lesssim 6°$ for all the cases presented here. Deviations from this simple approximation for electron refraction from copper surfaces may have been observed by Williams *et al.*[20] However, in our studies the sensitivity of the predicted spectra to emission angle was found to be rather low, probably because of the large size of the electron acceptance aperture, and thus an error of even a few degrees in the estimation of the electron refraction should not change the results appreciably.

B. Inclusion of momentum broadening in the final state

The second calculation method differed from the above only in that the requirement of strict $\vec{k}$ conservation for a transition was relaxed to account for certain sources of uncertainty in the final-state momentum.[12,23] This effect was first discussed in detail by Feibelman and Eastman.[23] In this work, the effect of the finite electron mean free path is accounted for by introducing a complex component in the momentum along the surface *normal*, resulting in an uncertainty or smearing in the final-state momentum normal to the surface. However, the discussion in Ref. 23 is limited to a first-order description of the photoemission process, which implies that smearing in the final-state momentum is small. In the case of a high degree of damping of final-state wave functions due to various inelastic processes, it is physically reasonable to limit the final-state wave function in space in a three-dimensional way. This could cause a broadening of the final-state momentum not only normal to, but also parallel to, the surface. In general, final-state momentum broadening is incorporated in our calculations as follows: For a given free-electron final state $\vec{k}^f$, we allow transitions to all final states with wave vector $\vec{k}^f$ and energy $E^f(\vec{k}^f) = \hbar^2|\vec{k}^f|^2/2m$ which satisfy

$$\vec{k}^f = \vec{k}^i + \vec{g} + \vec{k}_{\hbar\omega} + \Delta\vec{k}$$

and the energy conserving delta function in Eq. (1). $\Delta\vec{k}$ is here swept over some range, as described below. The maximum magnitude $|\Delta\vec{k}|_m$ can be obtained from the uncertainty principle, and, for a high damping region with mean free paths lying approximately between 3 and 5 Å, this gives $|\Delta\vec{k}|_m \approx (0.11-0.06)2\pi/a$ for copper with a lattice constant a. However, accurate values for the mean free path in copper at these energies are unfortunately not available.[21] In order to test various kinds of $\Delta\vec{k}$ broadenings, we have used three approximations: (1) $\Delta\vec{k}$ is along the surface normal only, i.e., $\Delta\vec{k} = \Delta\vec{k}_\perp$ and the range is $\pm|\Delta\vec{k}|_m$, (2) $\Delta\vec{k}$ is along the direction of the final-state wave vector, i.e., $\Delta\vec{k} \| \vec{k}^f$ and the range is $\pm|\Delta\vec{k}|_m$, and (3) $\Delta\vec{k}$ produces an isotropic broadening incorporated by allowing all $\Delta\vec{k}$'s within a cube of $2|\Delta\vec{k}|_m \times 2|\Delta\vec{k}|_m \times 2|\Delta\vec{k}|_m$. These three methods were tested by comparing theoretical results with $|\Delta\vec{k}|_m = (0.00-0.40)2\pi/a$ against experimental spectra. Method (3) was found to be inadequate because of an overestimation of the broadening along the plane perpendicular to $\vec{k}^f$. This is reasonable, since the group velocity of the final-state electron is along $\vec{k}^f$, so that spatial limitation due to electron inelastic scattering should be much weaker along the directions perpendicular to $\vec{k}^f$ as compared to parallel to $\vec{k}^f$. The differences in broadened spectra using methods (1) and (2) were not significant even for non-normal emission, probably because of the large electron acceptance aperture, and thus only spectra with $\Delta\vec{k}_\perp$ broadening are reported here. In various comparisons between theoretical and experimental results to be discussed, it has been found that a comparatively large $|\Delta\vec{k}_\perp|$ of $0.30(2\pi/a)$ gives the best agreement, and this is the value used in most of the theoretical spectra with momentum broadening. Of course, the momentum broadening depends on the kinetic energy of the photoemitted electrons, but it has been found that the calculated curves are not very sensitive to slight changes in $\Delta\vec{k}_\perp$ except for a few special cases which will be discussed in Sec. IV.

The results obtained by both calculation procedures have finally been broadened by a Gaussian of 0.4 eV FWHM to simulate approximately the instrumental contributions.

C. Discussion of model and phonon effects

Since the direction of $\vec{k}^f$ (in the extended zone) is known from the geometry of the system after

an allowance for surface refraction, there is a unique value of $\vec{g}$ which by $\vec{k}$ conservation projects this point into the Brillouin zone (BZ) to a unique value of $\vec{k}^i$ (Fig. 2). Thus, by choosing a suitable combination of photon energy and emission direction, it is possible to select a value of $\vec{k}^f$ that is projected back to *any* desired $\vec{k}^i$ point in the three-dimensional Brillouin zone. In the present work, the same set of high-symmetry zone points could thus be selected in two photon-energy ranges: one corresponding to a high surface-sensitive region around 70–100 eV and other corresponding to a region below 60 eV for which electron attenuation lengths should be somewhat longer.[21] In what follows, we express all wave vectors in normalized Cartesian components as $(k_x, k_y, k_z)2\pi/a$.

In the simplest view of the model used here, angle-resolved energy-distribution curves (AREDC's) obtained from the same symmetry points should be equivalent, but in fact there are several reasons why the experimental spectra may differ in fine details:

(1) Because of the finite experimental angular resolution *and* the need to rigorously conserve energy, the observed $\vec{k}^f$ values are found to lie within an approximately rectangular "box" in the extended zone that has a relatively small dimension along the mean emission direction. For example, emission from the X point $[\vec{k}^i = (0,0,-1)2\pi/a]$ in the three-dimensional BZ at a photon energy of 97.3 eV can be obtained with $\vec{g} = (0,0,4)2\pi/a$ and with emission normal to the surface ($\theta = 90°$, $\phi = 0°$). For emission at these conditions from the occupied valence states spanning an energy range from the Fermi level (E_F) to 9.0 eV below E_F, the mean value of $|\vec{k}^f|$ is $3.03(2\pi/a)$ and the $\vec{k}^f$ values lie within a box which has dimensions of $[0.53(2\pi/a) \times 0.64(2\pi/a)]$ perpendicular to $\vec{k}^f$ $\times 0.14(2\pi/a)$ parallel to $\vec{k}^f$. Photoemission from an equivalent symmetry point X can also be obtained by selecting $\hbar\omega = 52$ eV, which requires $\vec{g} = (2,0,2)2\pi/a$ and emission non-normal to the surface at $\theta = 58.7°$ and $\phi = 0°$. At these settings, the mean $|\vec{k}^f|$ is $2.27(2\pi/a)$ and the box dimensions are $[0.40(2\pi/a) \times 0.48(2\pi/a)] \times 0.19(2\pi/a)$. Also, the orientation of this box relative to the BZ is different for non-normal emission. Thus one would expect to find at least slight differences in the AREDC's from these equivalent points in the three-dimensional BZ, even within the context of the simple direct-transition-model calculations performed here.

(2) The change in the mean free path with energy may cause different degrees of momentum broadening in different spectra as discussed above, and also later in connection with specific spectra for the highly surface-sensitive region.

(3) As photon energies are increased, the increasing $\vec{g}$ vectors involved in the excitation could change the contribution of phonon-assisted indirect transitions, as first suggested by Shevchik.[16] The percentage of pure direct transitions remaining can be estimated from the Debye-Waller factor $\exp(-\frac{1}{3}\langle U^2\rangle g^2)$, where $\langle U^2\rangle$ is the mean-squared atomic displacement in the lattice. For example, for emission from the two equivalent X points discussed above at photon energies of 97.3 eV with $\vec{g} = (0,0,4)2\pi/a$ and 52 eV with $\vec{g} = (2,0,2)2\pi/a$, the Debye-Waller factors are 0.74 and 0.86, respectively (Table I). Thus, 26% of the transitions at 97.3 eV involve some kind of phonon-broadening in $\vec{k}^f$ and $\vec{k}^i$, whereas at 52 eV this is only 14%.

(4) Matrix-element effects such as: (a) Changes

TABLE I. Various parameters relating to the spectra considered here, including Debye-Waller factors for estimating the percentage of pure direct transitions remaining unperturbed by phonon effects.

$\hbar\omega$ (eV)	θ	ϕ	BZ point	$\vec{k}^i$ $(2\pi/a)$	$\vec{g}$ $(2\pi/a)$	$\exp(-\frac{1}{3}\langle U^2\rangle g^2)$
40.7	90°	0°	Γ	(0,0,0)	(0,0,2)	0.929
119.8	62.6°	45°	Γ	(0,0,0)	(1,1,3)	0.812
52.7	90°	0°	Δ	(0,0,0.25)	(0,0,2)	0.929
66.2	90°	0°	Δ	(0,0,0.5)	(0,0,2)	0.929
81.0	90°	0°	Δ	(0,0,0.75)	(0,0,2)	0.929
89.0	90°	0°	Δ	(0,0,0.88)	(0,0,2)	0.929
105.9	90°	0°	Δ	(0,0,−0.88)	(0,0,4)	0.745
97.3	90°	0°	X	(0,0,−1)	(0,0,4)	0.745
97.3	36.2°	26.6°	X	(0,1,0)	(2,0,2)	0.863
52.0	58.7°	0°	X	(1,0,0)	(2,0,2)	0.863
100.1	80°	0°	W	(0.5,0,1)	(1,1,3)	0.812
54.9	54.5°	26.6°	W	(1,0.5,0)	(2,0,2)	0.863

in the parities of the initial- and final-state wave functions with respect to a mirror plane, together with changes in the orientation of the polarization vector $\vec{A}$ relative to that mirror plane which could introduce significant intensity variations due to matrix elements and selection rules.[33-35] (b) More subtle $\hbar\omega$ dependence of matrix elements which could also influence the comparison between AREDC's from equivalent symmetry points in the three-dimensional BZ.[9,30]

(5) In addition, surface photoemission processes such as surface d-band narrowing, surface umklapp scattering, and emission from surface states may be important.[2,12,22-27] The roles of these effects will be discussed in more detail in connection with various specific spectra in Sec. IV.

We conclude this theoretical introduction by noting that it is not our intention here to discuss or compare our experimental results with other inherently more accurate models of photoemission that include, for example, multiple scattering in the final state and a detailed calculation of all relevant matrix elements.[36] Rather we will attempt to explore the degree to which a physically very simple and transparent model can be used as a first-order description of the data, but it is clear that comparisons to more accurate calculations are very desirable in the future. However, calculations at this higher level of accuracy are in any case not yet available for most of the experimental conditions we have employed here.

IV. RESULTS AND DISCUSSIONS

Figure 3 shows spectra which should, according to this direct-transition model, originate primarily from the Γ point [$\vec{k}^i = (0,0,0)2\pi/a$] in the three-dimensional BZ; the $\vec{g}$ vectors involved are mostly $(0,0,2)2\pi/a$ for 40.7 eV and $(1,1,3)2\pi/a$ for 119.8 eV. The results for 119.8 eV furthermore correspond to non-normal emission ($\theta = 62.6°$), whereas 40.7 eV is normal. Experimental spectra are also shown for two different polarization orientations: $\alpha = 9°$ (upper curves) and $\alpha = 42°$ (lower curves). All of the spectra we will present have been normalized to the same constant maximum height. There is very good agreement between experiment and theory as to the positions of the two dominant close-lying peaks labeled 2, 3 and 5, 6. Both $\Gamma_{25'}$ states (associated with

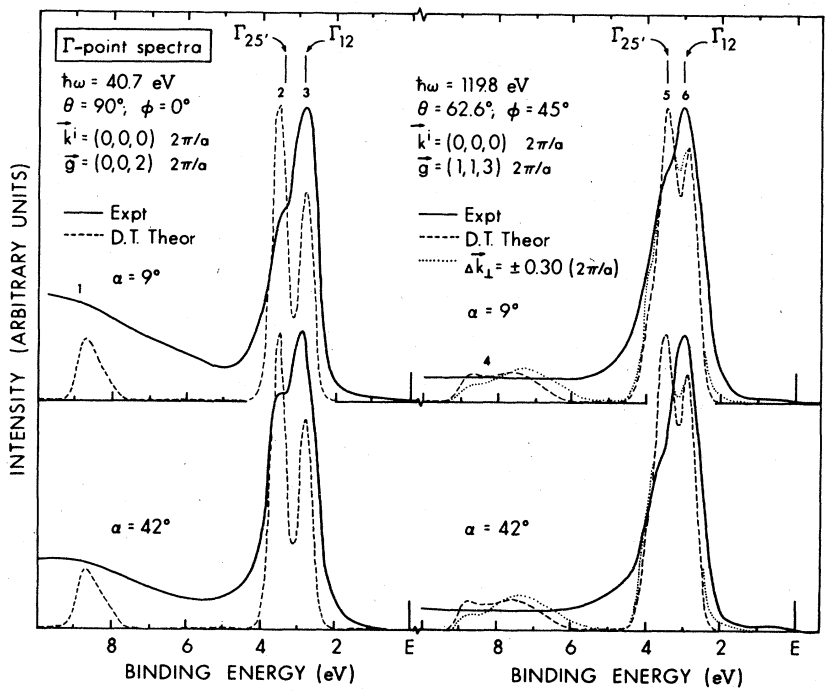

FIG. 3. Experimental photoemission spectra originating primarily from the Γ point in the three-dimensional BZ obtained at two different sets of conditions as to photon energies, electron directions, and polarization orientations (the solid curves) are compared to the results of two direct-transition-model calculations (the dotted curves). For each case, the first theoretical curve (---) was derived by using the first simple direct-transition model described in the text. The second curve (···) includes a momentum broadening in the final-state wave vector normal to the surface [$|\Delta\vec{k}_\perp| = 0.30(2\pi/a)$] and is shown only for spectra obtained in what is expected to be a high-surface-sensitivity or low-mean-free-path region. All curves have been normalized to the same maximum height.

the peaks labeled 2 and 5) corresponding to atomic d-orbital functions with primarily t_{2g} symmetry (xy, yz, xz) and Γ_{12} states (peaks 3 and 6) with primarily e_g symmetry (z^2, x^2-y^2) (Ref. 37) are clearly observed in the experimental AREDC's. The predicted and observed separations of the peaks 2,3 and 5,6 are within 0.1 eV of one another. The fact that peaks 1 and 4 predicted at higher binding energies of 6.0–9.0 eV are not clearly observed experimentally is easily explained in terms of matrix-element effects. That is, tight-binding calculations indicate that these peaks correspond to states with a very high percentage of plane-wave or s-like character. Such character is expected to lead to much smaller matrix elements than d-like character. For example, purely atomic cross-section calculations have been performed for copper over the energy range of interest here[38] using the Manson-Cooper central potential model.[39] These yield σ_{4s}/σ_{3d} ratios per electron that vary smoothly over the range $40 \leq \hbar\omega \leq 140$ eV, with values of 0.042 at 40 eV, 0.028 at 80 eV, and 0.027 at 120 eV. It is also significant that the AREDC's obtained from equivalent BZ points but with normal and non-normal emission are similar in shape, except that peaks 5 and 6 are less well resolved at $\hbar\omega = 119.8$ eV. Possible reasons for the poorer resolution at higher photon energy are the larger size of the electron acceptance region in $\vec{k}^f$ space [$0.58(2\pi/a) \times 0.69(2\pi/a) \times 0.12(2\pi/a)$ at 119.8 eV compared to $0.35(2\pi/a) \times 0.42(2\pi/a) \times 0.22(2\pi/a)$ at 40.7 eV]; the higher degree of momentum broadening in the final-state wave vector for 119.8 eV, as this energy should correspond to a more highly surface-sensitive region; an increase in the monochromator contribution to the resolution (0.01 eV at $\hbar\omega = 40.7$ eV compared to 0.12 eV at $\hbar\omega = 119.8$ eV); and finally, the lower Debye-Waller factor at higher photon energies (0.92 at 40.7 eV compared to 0.82 at 119.8 eV), which results in a larger fraction of phonon assisted indirect transitions[16] (cf. Table I). However, the very close resemblance between AREDC's obtained with different photon energies and electron emission directions is a strong first indication from our results that the simple direct-transition model is applicable to both normal *and* non-normal transitions.

The variations observed in the AREDC's of Fig. 3 with changes in orientation of the polarization vector $\vec{A}$ can be qualitatively expained using symmetry arguments. Hermanson[33] has shown that, in the absence of spin-orbit coupling, only final states with *even* parity can be observed in photoemission measurements performed either normal to the surface or confined to a mirror plane containing the surface normal. For an allowed transition, the integrand in the matrix element $\langle\phi^f|\vec{A}\cdot\vec{\nabla}|\phi^i|$ must have even parity. Thus, in a photoemission experiment where the polarization vector $\vec{A}$ is parallel to a mirror plane (i.e., $\vec{A}\cdot\vec{\nabla}$ is of even parity) and also the electron emission is either normal to the surface or confined to the mirror plane, nonzero matrix elements result only from initial states with *even* parity. A further consideration of the selection rules involved shows that, for normal emission from the (001) surface with the components of the polarization vector $\vec{A}$ parallel to the [100], [010], and [001] axes, emission will be allowed from initial states with Δ_5, Δ_5, or Δ_1 symmetries, respectively;[33] Δ_2 or Δ_2' states can never be excited for normal emission. Although these selection rules are not strictly applicable to any of our results because of the finite acceptance aperture and the experimental geometry (for which $\vec{A}$ cannot be made exactly perpendicular to the surface, but rather only within 9° of the surface normal, as shown in Fig. 1), they can be used qualitatively in comparing certain spectra from the same states excited with different polarizations. It should also be noted that, for general orientations of $\vec{A}$ and the emission direction, strong symmetry selection rules will not exist, but the choices of $\vec{A}$ and $\vec{k}^f$ will change the matrix elements.[34,35] If we consider now the experimental results, the spectra from the Γ point at $\hbar\omega = 40.7$ eV with emission along the normal direction (where strict selection rules are very nearly applicable in our experimental geometry) are in accordance with the known parities of the initial states involved in the excitations. That is, the peak labeled 3 (Γ_{12}) which mainly consists of transitions from a $z^2(\Delta_1)$ state of e_g symmetry is clearly enhanced as expected at $\alpha = 9°$ where there is a larger component of $\vec{A}$ along the surface normal. No such selection rules are applicable for non-normal emission from Γ at $\hbar\omega = 119.8$ eV, and thus the change observed in the relative height of the leading peaks due to the change in the orientation of $\vec{A}$ can only be attributed to a change in matrix elements.

Figure 4 shows AREDC's obtained at normal emission ($\theta = 90°$, $\phi = 0°$) with $\alpha = 42°$ and by selecting suitable photon energies so as to obtain direct-transition emission primarily from specific groups of states lying along the Γ-Δ-X direction in the three-dimensional BZ. The photon energy, the $\vec{g}$ vector, and the principal initial $\vec{k}$ point being excited in the three-dimensional BZ are also given in the figure. In general, there is good agreement between simple direct-transition theory and experiment as to peak positions and general trends in intensity changes with $\hbar\omega$, although there is some disagreement in fine structure, especially

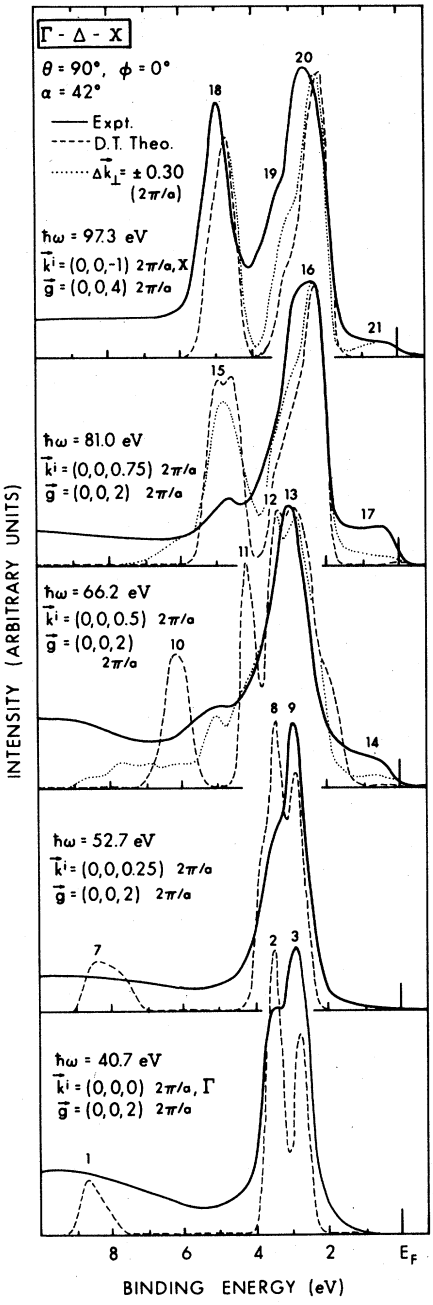

FIG. 4. Photoemission spectra obtained at normal emission by exciting various initial states lying along the Γ-Δ-*X* direction in the three-dimensional BZ are compared with direct-transition theoretical calculations of two types [simple and with an additional $|\Delta\vec{k}_\perp|$ broadening of $0.3(2\pi/a)$]. Note that the peaks labeled 10 and 11 predicted by the simple direct-transition theory have merged into one peak in the theoretical spectrum with momentum broadening, in excellent agreement with the experiment.

for $\hbar\omega$ near 66.2 eV. The spectrum obtained at $\hbar\omega = 52.7$ eV by excitation of initial states with $\vec{k}^i = (0, 0, 0.25)2\pi/a$ is quite similar to the spectrum from the Γ point because the *d* bands are very flat in this $\vec{k}$ interval. Once again, the peaks labeled 1 and 7 predicted at higher binding energies of 7-9 eV have essentially 100% plane-wave character and are not observed experimentally because of much smaller relative matrix elements. However, one disagreement between the simple direct-transition model and experiment concerns the relative intensity of the weak *s*-*p*-*d* band emission between E_F and 2 eV (peaks labeled 14, 17, and 21) which have not been predicted in the simple theoretical model. Another point of disagreement arises for the spectrum obtained at $\hbar\omega = 66.2$ eV with $\vec{k}^i = (0, 0, 0.5)2\pi/a$, where theoretically predicted peaks at binding energies of 6.2 and 4.2 eV (labeled 10 and 11) arising from Δ_1 and Δ_2' states, respectively, are not experimentally observed, and instead a peak at approximately 5 eV is detected. Both of these disagreements can, however, be well explained qualitatively by noting that these spectra correspond to a highly surface-sensitive energy region where smearing in the final-state momentum should become significant.[2,12,22-25] Theoretical spectra obtained with a broadening in $\vec{k}^f$ of $|\Delta\vec{k}_\perp| = 0.3(2\pi/a)$ are in fact found to significantly improve the agreement between theory and experiment, as shown also in Fig. 4. As a result of this broadening, there is an appearance of significant intensity in the calculated spectra between E_F and 2 eV, and also the peaks labeled 10 and 11 have merged to one peak at ~5 eV that is in excellent agreement with the experimentally observed peak at the same energy. This suggests that there is a significant broadening in $\vec{k}^f$ which appears to exist for all the spectra taken in the highly surface-sensitive region $\hbar\omega \approx 60$–110 eV.

To more fully explore the effect of such broadenings, Fig. 5 shows AREDC's calculated for emission from initial states $\vec{k}^i = (0, 0, 0.5)2\pi/a$ with $\hbar\omega = 66.2$ eV as a function of momentum broadening in the final state ($\Delta\vec{k}_\perp$). A broadening of $|\Delta\vec{k}_\perp| \approx (0.2$–$0.3)2\pi/a$ in the normal component $\vec{k}^f$ is required to obtain the best agreement between theory and experiment. This is significantly larger than, although of the same order as, the values estimated previously on the basis of inelastic scattering of $|\Delta\vec{k}_\perp| \approx 0.1(2\pi/a)$ (e.g., see Sec. IIIB and Fig. 6 in Ref. 23). This suggests that the improved agreement between theory and experiment by introducing $\Delta\vec{k}_\perp$ broadening should not be understood only in terms of a short mean free path of the final-state electron. As one other possible source of effective broadening, it should be noted that Himpsel *et al.*[40] have recently re-

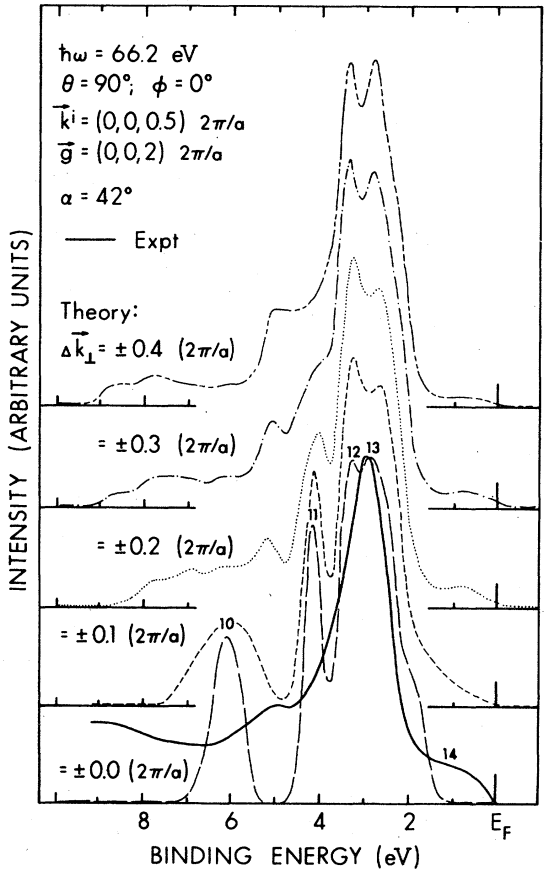

FIG. 5. Calculated photoemission spectra for $\hbar\omega = 66.2$ eV and $\vec{k}^i = (0, 0, 0.5)2\pi/a$ with different degrees of momentum broadening in the final state are compared with the corresponding experimental curve (solid line). A momentum broadening of $|\Delta\vec{k}_\perp| \approx 0.2-0.3(2\pi/a)$ is required to obtain optimum agreement between theory and experiment.

ported angle-resolved photoemission measurements for Cu(001) for an experimental geometry very similar to that of Fig. 4 and for normal emission. Based upon an analysis of these results, it has been suggested[40] that additional non-free-electron final states close to, but separated by as much as 10 eV from the free-electron final states exist at $E^f \approx 60$ eV. However, the overall transition probabilities to such final states from the s-p band just below E_F are about one order of magnitude less than those of the principal free-electron transition. These results also show that transitions to final states presumably close to free-electron final states in certain cases have intensity peaks as wide as a FWHM of ~12 eV if the excitation energy is swept. Such large FWHM's thus also qualitatively explain the necessity of the large $|\Delta\vec{k}_\perp|$ in our model calculation. Another possible cause of such effects may be that phonon-assisted nondirect transitions with small phonon wave vectors result in "quasidirect" transitions with an additional effective broadening. This is analogous to the thermal diffuse scattering peak that is centered on the Bragg (direct transition) peaks in x-ray or electron diffraction[41] and its effect is not adequately included in a simple Debye-Waller analysis of vibrational motion. So, phonons may introduce additional broadening and further help to explain why a large empirical $\Delta\vec{k}_\perp$ results.

To continue with the discussion of Fig. 4, the photoemission spectrum obtained at $\hbar\omega = 81$ eV with $\vec{k}^i = (0, 0, 0.75)2\pi/a$, shows a separation of Δ_1, Δ_2' and Δ_5, Δ_2 states (associated with the peaks labeled 15 and 16, respectively) as predicted rather well by the unbroadened direct-transition theory, but with some disagreement in the intensities of peaks labeled 15 and 17 that are involved. The theoretical spectrum with relaxation in $\vec{k}^f$ improves the agreement by suppressing peak 15, increasing the FWHM of peak 16, and also by predicting additional intensity for emission between E_F and 2 eV. In addition, the low observed intensity of peak 15 may be explained by noting that this peak consists of contributions partly from a Δ_2' state which is symmetry forbidden and partly from a Δ_1 state which has about 25% plane-wave character. (In certain cases, we have used wave functions generated by an empirical tight-binding program due to Smith and coworkers[42] to assign orbital characters.) The experimental valence-band spectrum at a photon energy of 97.3 eV corresponding to states near the X point in the three-dimensional BZ is in very good agreement with theory with $\Delta\vec{k}_\perp$ broadening, although a small displacement of peak positions by ~0.3 eV is evident.

Figure 6 shows spectra originating primarily from different X points in the three-dimensional BZ excited with different photon energies (or equivalently, different $\vec{g}$ vectors) and with both normal and non-normal emission. The spectra are shown for two different orientations of the polarization vector $\vec{A}$: $\alpha = 9°$ and $42°$ (cf. Fig. 1). Note also that 2 out of 3 sets of spectra involve the same photon energy of 97.3 eV. There is overall agreement between simple direct-transition theory and experiment as to the dominant two-peak structure observed for all cases, but with discrepancies as to the positions and widths of a few experimental peaks. The spectra obtained at the higher photon energy of 97.3 eV have substantially larger widths than spectra obtained at $\hbar\omega = 52$ eV, and this width difference is not fully predicted by the simple direct-transition model. Once again, a less obvious point of disagreement concerns the relatively low intensity predicted for emission

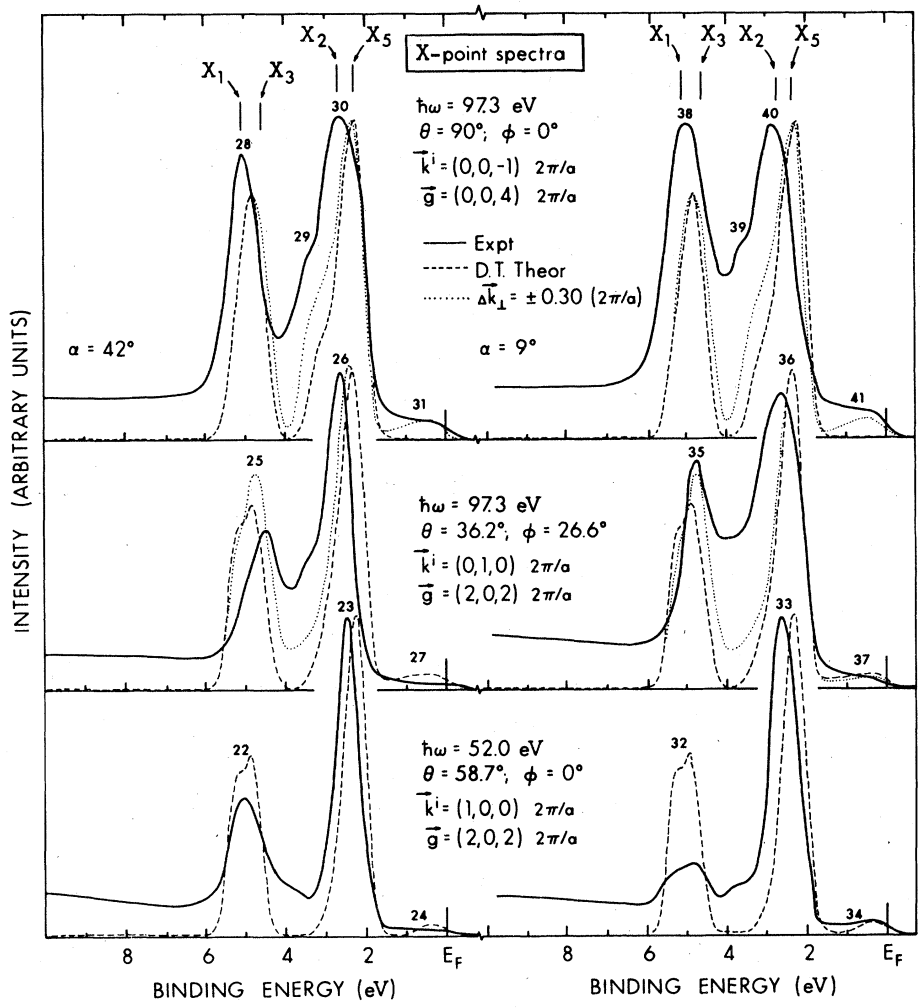

FIG. 6. As for Fig. 3, but with initial states near three equivalent X points in the three-dimensional BZ.

between E_F and 2 eV for the peaks labeled 31 and 41. In addition, the photoemission spectra obtained from initial states at the X point $\vec{k}^i = (0,1,0)2\pi/a$, $\hbar\omega = 97.3$ eV with $\alpha = 9°$ and 42°, show a shift in the positions of the high binding-energy peaks (labeled 25 and 35) which is not fully predicted by the simple direct-transition model. By including the empirically derived momentum broadening of $\pm (0.30)2\pi/a$ in the theoretical spectra there is very good agreement for the intensity just below the Fermi level (peaks 31 and 41) and the shift in the high binding-energy peaks 25 and 35 is also qualitatively predicted, thus providing a considerable improvement in the agreement with experiment. A further possible explanation for certain experimentally observed shifts for peaks 25 and 35 can be made by using symmetry arguments. At normal emission and with $\vec{A}$ in the {001} mirror plane, only bands of X_1 and X_5 symmetries are allowed to contribute to the photoemission intensity.[33] This would thus apply to the normal emission spectrum at 97.3 eV. When neither electron emission nor $\vec{A}$ is in a high-symmetry plane, these selection rules are broken and all states become allowed. This would apply to the spectra for non-normal emission at 97.3 eV with $\theta = 36°$ and $\phi = 26.6°$ and would tend to move the two peaks of the spectrum closer together[13,37] as compared with the case where only the X_1 and X_5 states are allowed. It should also be pointed out that changing the polar angle from $\theta = 90°$ to 36° reduces the relative electron escape depth (which will be proportional to $\sin\theta$) by only a factor of 0.59, and thus, this does not seem sufficient to explain the shift in the peaks 25 and 35 as being surface associated. The results shown in Fig. 6 also clearly follow the symmetry selection rules for spectra obtained for the X point

with normal emission and with the different polarization angles of $\alpha = 9°$ and 42°. The high binding-energy peak (labeled 38) consisting mainly of X_1 contributions is enhanced in intensity as expected when the polarization angle is changed from $\alpha = 42°$ to 9°, where it is to the first order the only symmetry allowed to contribute.[33] For $\alpha = 9°$, there is also an expected increase in intensity between E_F and 2 eV (labeled 41) where the states have mainly Δ_1 symmetry and are allowed due to momentum broadening in the final state. The rather large FWHM's of the peaks labeled 29, 30 and 39, 40 can also be primarily explained by including momentum broadening in the theoretical spectra, and calculations after broadening do show stronger shoulders 29 and 39 in better agreement with observations. Certain small remaining discrepancies (for example, comparing shapes and FWHM's of peak 26 with 29, 30) might be explained by noting that one set of data has been excited mostly with $\vec{g} = (0,0,4)2\pi/a$, as compared to spectra at the same energy but non-normal emission which involve $\vec{g} = (2,0,2)2\pi/a$. Thus, the larger $|\vec{g}|$ value in the former case leads to more phonon-assisted $\vec{k}$ smearing[16] for X-point emission along the normal direction as compared to non-normal emission, even though both are excited with the same $\hbar\omega = 97.3$ eV (cf. Debye-Waller factors in Table I). Phonon-assisted indirect transitions are further discussed in connection with Fig. 7.

The spectra of Fig. 6 obtained from initial states near the X point $\vec{k}^i = (1,0,0)2\pi/a$ and excited with $\hbar\omega = 52$ eV show peaks labeled 22, 23, 24, 32, 33, and 34 with overall widths and position that are well predicted by the simple direct-transition theory. The theoretical spectra at $\hbar\omega = 52$ eV do not need a significant degree of momentum broadening to agree with experiment, as is expected because the energy corresponds to both a higher mean free path[21] and a smaller $\vec{g}$ value. The only significant discrepancy noted between theory and experiment is the low intensity of the observed peak 32 as compared to the theory. This can be explained in terms of simple plane-wave matrix-element calculations[9,43] which should be more applicable for $\vec{A}$ along the near-normal direction for which $\vec{A}$ is approximately parallel to $\vec{k}^f$,[44] and a theoretical spectrum obtained by including such matrix elements in addition to the $\vec{k}$-conservation requirement is found to show a substantial decrease in the intensity of peak 32 for this case. In general, however, we stress that the inclusion of such plane-wave matrix elements for arbitrary geometries yields very poor agreement with the experiment, as has been previously discussed by Wagner *et al.*[9]

Figure 7 shows AREDC's originating in normal emission primarily from two symmetry-equivalent points along the Δ line [$\vec{k}^i = (0,0,0.88)2\pi/a$ and $\vec{k}^i = (0,0,-0.88)2\pi/a$] which lie close to, but on opposite sides of, the X point in an extended-zone scheme. These were excited with photon energies of 89.0 and 105.9 eV and involve $\vec{g} = (0,0,2)2\pi/a$ and $\vec{g} = (0,0,4)2\pi/a$, respectively. There are significant differences in the experimental spectra from these equivalent points which can mainly be attributed to the difference in $\vec{g}$ vectors involved in excitation. That is, since the average kinetic energies of the photoemitted electrons in these spectra are quite similar and should correspond to about the same mean free path, contributions to these spectra from inelastic momentum broadening should be approximately the same. The theoretical spectra of Figs. 7 with momentum broadening do show an increase in FWHM from 0.7 to 1.1 eV of the peak at a binding energy of about 2.5 eV. This fully agrees with the experimentally observed FWHM of the composite peak labeled 43, 44 obtained at $\hbar\omega = 89.0$ eV with $\vec{g} = (0,0,2)2\pi/a$, but does not fully account for the large 1.9 eV FWHM of peaks 47, 48 at 105.9 eV and excited with $\vec{g} = (0,0,4)2\pi/a$. The difference

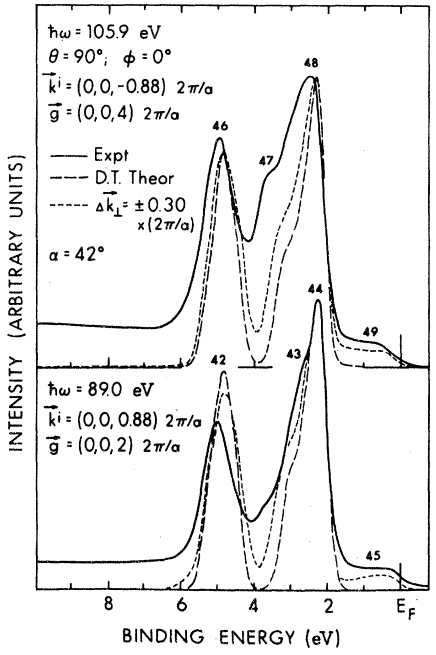

FIG. 7. Photoemission spectra originating primarily from two groups of initial-state symmetry equivalent in $\vec{k}^i$ and lying along the Δ line are compared with direct-transition theoretical curves. These spectra are excited with photon energies of about equal surface sensitivity at 89 and 105.9 eV, but the transitions utilize two different g vectors, $\vec{g} = (0,0,2)2\pi/a$ and $\vec{g} = (0,0,4)2\pi/a$, respectively.

in size of the acceptance region in $\vec{k}$ space for these spectra is also less than 10% and it is not sufficient to account for the change being observed; in fact, such effects have already been explicitly included in the theoretical curves presented. Therefore, the remaining differences in the above spectra can mainly be attributed to the change in $\vec{g}$ vector which also changes the number of phonon-assisted indirect transitions through a change in the Debye-Waller factor, as first discussed by Shevchik.[16] According to this model, in the spectrum at room temperature excited with $\vec{g} = (0,0,2)2\pi/a$, only 7% of the transitions are phonon-assisted indirect (Debye-Waller factor = 0.93) whereas this number increases to 26% with $\vec{g} = (0,0,4)2\pi/a$ (Debye-Waller factor = 0.74, as shown in Table I). Although it is very hard to make a quantitative estimate of the phonon-assisted smearing present in the experimental spectra of Fig. 7, the type of effect observed is still qualitatively compatible with this theoretical prediction. The particular spectra obtained thus permit separating out the effects due to phonon-induced smearing from other effects such as momentum broadening in the final-state wave vector. The use of temperature-dependent measurements should permit more clearly distinguishing such phonon effects, as has recently been demonstrated in angle-resolved XPS by Hussain *et al.*[19]

Figure 8 shows results obtained from two equivalent initial bulk states near W symmetry points [$\vec{k}^i = (1, 0.5, 0)2\pi/a$ and $\vec{k}^i = (0.5, 0, 1)2\pi/a$ at $\hbar\omega = 54.9$ and 100.1 eV, respectively] and with polarization angles of $\alpha = 9°$ and 42°. There is general agreement between simple direct-transition theory and experiment, but with some differences in the positions of the leading peaks labeled 51, 53, and 60 at binding energies between 2 and 3 eV. The emission at this energy arises mainly from close-lying W_1 and W_1' states of e_g and t_{2g} symmetry, respectively.[13,37] By including momentum broadening in the theoretical spectra at $\hbar\omega = 100.1$ eV, some separation in the components of this leading peak is clearly seen, and this assists in explaining certain discrepancies. The spectra show significant changes in peak intensity due to changes in the direction of the polarization vector $\vec{A}$ which enable the unambiguous assignment of these peaks to certain initial states. A comparison of the W-point spectra for $\alpha = 9°$ at $\hbar\omega = 54.9$ and 100.1 eV clearly shows that for electron emission and polarization vector in the {010} mirror plane ($\phi = 0°$) the contribution from the symmetry-forbidden W_1 state of t_{2g} symmetry is greatly suppressed, whereas at 54.9 eV when both $\vec{A}$ and electron emission direction are not in a high-symmetry plane, the strict symmetry selection rules are broken, thereby allowing emission from all states. Also,

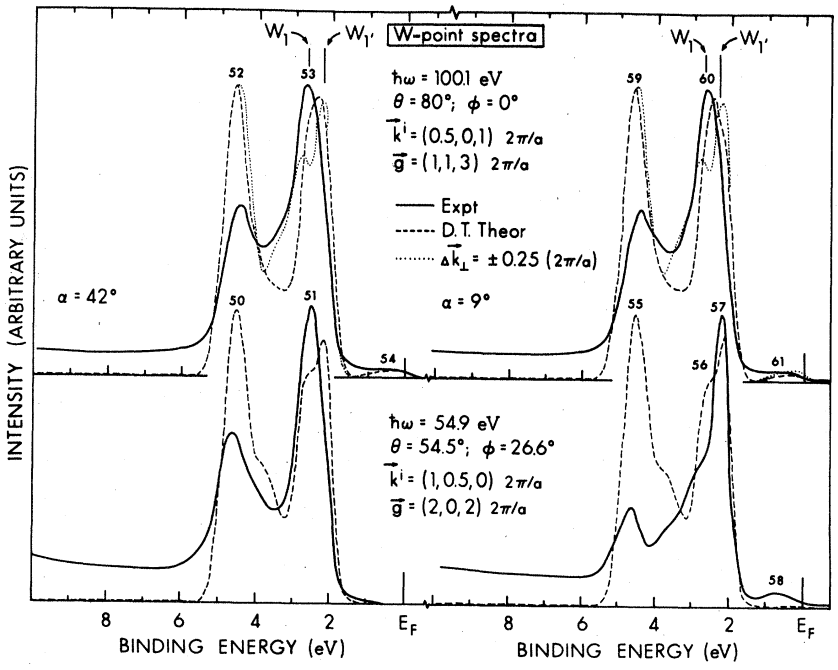

FIG. 8. As for Fig. 3, but with initial states near two equivalent W points in the three-dimensional BZ. Note the shift of peaks labeled 51 and 57 when the polarization orientation is changed from 42° to 9°.

if we compare the two W-point spectra excited with $\hbar\omega = 54.9$ eV and the two different polarization orientations, the change in polarization produces a marked peak shift of the higher binding-energy peak. (The two identical theoretical spectra can be used to gauge relative peak positions between the experimental spectra.) Since the structure is mainly peaked at lower binding energy for $\alpha = 9°$ (peak 51), states of W_1' (t_{2g}) symmetry dominate the emission for this polarization, whereas for $\alpha = 42°$, states of W_1 (e_g) symmetry are dominant (peak 57).

Finally, we note that three types of surface-associated effects, namely surface d-band narrowing,[25,26] surface umklapp scattering,[12,22] and surface states[26,27,45] do not appear to represent highly significant effects in any of our spectra, although of course they could account for certain remaining differences between experiment and theory. We also do not agree with a recent interpretation of the photoemission spectra from copper in terms of a surface density of states, for example, as recently proposed by Verges *et al.*[27]

V. CONCLUSIONS

The experiments and calculations presented here clarify the role of various bulk effects present in angle-resolved photoemission spectra of copper (001) obtained in the energy range 40–120 eV. Our results show that a simple direct-transition model with constant matrix elements provides a good first-order description of the spectra not only for *normal* emission but also for *non-normal* emission. Thus, by utilizing emission both normal and non-normal to one crystal-surface orientation along with the direct-transition model, it has been possible to select initial states near various symmetry points in the three-dimensional BZ for study. For certain spectra in the energy range 60–100 eV, an additional empirical momentum broadening is needed to obtain optimum agreement with experiment. This broadening could be due to short electron attenuation lengths, complexities in the final-state bands, and/or phonon-assisted nondirect transitions. These results suggest that one must be very careful in using angle-resolved photoemission in this energy region to map the three-dimensional band structure. The enhancement of phonon-assisted nondirect transitions in the photemission spectra due to an increase in $\vec{g}$ vector is also observed. Finally, we have further demonstrated the use of different polarization orientations and symmetry-based selection rules for assigning contributions to the emission from various initial states.

ACKNOWLEDGMENTS

We would like to thank the Lindau and Spicer Research Groups at Stanford University for the use of equipment and also for useful discussions. Two of us (Z. H. and L. –G. P.) are grateful to the East-West Center in Honolulu and the Swedish National Science Research Council (NFR), respectively, for financial support. This work has been supported by the National Science Foundation (Grant No. CHE76-24506) and The Petroleum Research Fund. This work was performed at the Stanford Synchrotron Radiation Laboratory, which is supported by NSF Grant No. DMR 73-07692 A02, in cooperation with the Stanford Linear Acceleration Center.

---

*Present address: Materials and Molecular Research Division, Lawrence Berkeley Laboratory, University of California, Berkeley, California 94720.

†Present address: Department of Physics and Measurement Technology, Linköping University S-581 83 Linköping, Sweden.

‡Present address: Department of Chemistry, University of Utah, Salt Lake City, Utah 84112.

[1]For a review in the range $\hbar\omega < 25$ eV see D. E. Eastman, in *Vacuum Ultraviolet Radiation Physics*, edited by E. E. Koch, R. Haensel, and C. Kunz (Pergamon, Vieweg, 1974), p. 417.

[2]For a review in the range $30 \leq \hbar\omega \leq 200$ eV see D. A. Shirley, J. Stöhr, P. S. Wehner, R. S. Williams, and G. Apai, Phys. Scr. 16, 398 (1977).

[3]J. Stöhr, F. R. McFeely, G. Apai, P. S. Wehner, and D. A. Shirley, Phys. Rev. B 14, 4431 (1975).

[4]H. Becker, E. Dietz, N. Gerhardt, and H. Angermuller, Phys. Rev. B 12, 2084 (1975).

[5]P. O. Nilsson and L. Ilver, Solid State Commun. 17, 667 (1975); 18, 677 (1976).

[6]J. Stöhr, G. Apai, P. S. Wehner, F. R. McFeely, R. S. Williams, and D. A. Shirley, Phys. Rev. B 14, 5144 (1976).

[7]G. Apai, J. Stöhr, R. S. Williams, P. S. Wehner, S. P. Kowalczyk, and D. A. Shirley, Phys. Rev. B 15, 584 (1977).

[8]L. F. Wagner, Z. Hussain, C. S. Fadley, and R. J. Baird, Solid State Commun. 21, 453 (1977).

[9]L. F. Wagner, Z. Hussain, and C. S. Fadley, Solid State Commun. 21, 257 (1977).

[10]J. Stöhr, P. S. Wehner, R. S. Williams, G. Apai, and D. A. Shirley, Phys. Rev. B 17, 587 (1978).

[11]D. E. Eastman, J. A. Knapp, and F. H. Himpsel, Phys. Rev. Lett. 41, 825 (1978).

[12]P. Thiry, D. Chandesri, J. Lecante, C. Guillot, R. Pinchaux, and Y. Petroff, Phys. Rev. Lett. 43, 82 (1979).

[13]G. A. Burdick, Phys. Rev. 129, 138 (1963).
[14]J. F. Janak, A. R. Williams, and V. L. Moruzzi, Phys. Rev. B 11, 1522 (1975).
[15]N. V. Smith, Phys. Rev. Lett. 23, 1452 (1969); Phys. Rev. B 3, 1862 (1971).
[16]N. J. Shevchik, Phys. Rev. B 16, 3428 (1977).
[17]Z. Hussain, N. F. T. Hall, L. F. Wagner, S. P. Kowalczyk, C. S. Fadley, K. A. Thomson, and R. A. Dod, Solid State Commun. 25, 907 (1978).
[18]M. J. Sayers and F. R. McFeely, Phys. Rev. B 17, 3867 (1978).
[19]Z. Hussain, S. Kono, C. S. Fadley, and R. Connolly, Phys. Rev. Lett. 44, 895 (1980); and Z. Hussain, C. S. Fadley, S. Kono, and L. F. Wagner, Phys. Rev. B 22, 3750 (1980).
[20]R. S. Williams, P. S. Wehner, J. Stöhr, and D. A. Shirley, Surf. Sci. 75, 215 (1978).
[21]I. Lindau and W. E. Spicer, J. Electron. Spectrosc. Relat. Phenom. 3, 409 (1974); and M. P. Seah and W. A. Dench, Surf. Interf. Anal. 1, 2 (1979).
[22]B. Feuerbacher and R. F. Willis, J. Phys. C 9, 169 (1976).
[23]P. J. Feibelman and D. E. Eastman, Phys. Rev. B 10, 4932 (1974).
[24]M. Sagurton and N. V. Shevchik, Phys. Rev. B 17, 3859 (1978).
[25]J. B. Pendry and D. J. Titterington, Commun. Phys. 2, 31 (1977); M. Mehta and C. S. Fadley, Phys. Rev. B 20, 2280 (1979).
[26]D. G. Dempsey and L. Kleinman, Phys. Rev. B 16, 5356 (1977).
[27]J. A. Vergés and F. Yndurian, Solid State Commun. 99, 635 (1979).
[28]L.-G. Petersson, Z. Hussain, S. Kono, and C. S. Fadley, Solid State Commun. 34, 549 (1980).
[29]A. Savitzky and M. J. E. Golay, Anal. Chem. 36, 1627 (1964); and J. Steinier, Y. Termonia, and J. Deltour, *ibid.* 44, 1906 (1972).
[30]G. D. Mahan, Phys. Rev. B 2, 4334 (1970).
[31]P. O. Nilsson and N. Dahlbäck, Solid State Commun. 29, 303 (1979).
[32]T. A. Delchar, Surf. Sci. 27, 11 (1971).
[33]J. Hermanson, Solid State Commun. 22, 9 (1977).
[34]J. Anderson, G. J. Lapeyre, and R. J. Smith, Phys. Rev. B 17, 2436 (1978).
[35]N. V. Richardson, J. K. Sass, D. R. Lloyd, and C. M. Quinn, Surf. Sci. 80, 165 (1979).
[36]J. B. Pendry and J. F. L. Hopkinson, J. Phys. (Paris) C4, 142 (1978).
[37]See, e.g., J. F. Cornwell, *Group Theory and Electronic Energy Bands in Solids* (North-Holland, Amsterdam, 1969).
[38]S. M. Goldberg, C. S. Fadley, and S. Kono, J. Electron. Spectrosc. Relat. Phenom. (in press).
[39]S. T. Manson and J. W. Cooper, Phys. Rev. 165, 126 (1968).
[40]F. J. Himpsel and W. Eberhardt, Solid State Commun. 31, 747 (1979).
[41]See, e.g., B. E. Warren, *X-ray Diffraction* (Addison-Wesley, Reading, Mass., 1969); and J. B. Pendry, *Low-Energy Electron Diffraction* (Academic, London, 1974).
[42]N. V. Smith and L. F. Mattheiss, Phys. Rev. B 9, 1341 (1974).
[43]F. R. McFeely, J. Stöhr, G. Apai, P. S. Wehner, and D. A. Shirley, Phys. Rev. B 14, 3273 (1976).
[44]S. M. Goldberg, C. S. Fadley, and S. Kono, Solid State Commun. 28, 459 (1978).
[45]P. O. Gartland and B. J. Slagsvold, Phys. Rev. B 12, 4047 (1975).